Lattice Induced Short-Range Attraction between Like-Charged Colloidal Particles

Peng Liu,[1,2,3] Luhui Ning,[1,2,3] Yiwu Zong,[4] Fangfu Ye,[1,2,3,5,*] Mingcheng Yang,[1,2,5,†] and Ke Chen[1,2,5,‡]

[1]*Beijing National Laboratory for Condensed Matter Physics and Laboratory of Soft Matter Physics, Institute of Physics, Chinese Academy of Sciences, Beijing 100190, China*

[2]*School of Physical Sciences, University of Chinese Academy of Sciences, Beijing 100049, China*

[3]*Wenzhou Institute, University of Chinese Academy of Sciences, Wenzhou, Zhejiang 325001, China*

[4]*Frontiers Science Center for Synthetic Biology and Key Laboratory of Systems Bioengineering (Ministry of Education), School of Chemical Engineering and Technology, Tianjin University, Tianjin 300072, China*

[5]*Songshan Lake Materials Laboratory, Dongguan, Guangdong 523808, China*

(Received 24 November 2021; revised 13 April 2022; accepted 2 June 2022; published 30 June 2022)

We perform experiments and computer simulations to study the effective interactions between like-charged colloidal tracers moving in a two-dimensional fluctuating background of colloidal crystal. By a counting method that properly accounts for the configurational degeneracy of tracer pairs, we extract the relative probability of finding a tracer pair in neighboring triangular cells formed by background particles. We find that this probability at the nearest neighbor cell is remarkably greater than those at cells with larger separations, implying an effective attraction between the tracers. This effective attraction weakens sharply as the background lattice constant increases. Furthermore, we clarify that the lattice-mediated effective attraction originates from the minimization of free energy increase from deformation of the crystalline background due to the presence of diffusing tracers.

DOI: 10.1103/PhysRevLett.129.018002

Introduction.—Attractive interactions between like-charged colloidal particles have been repeatedly reported under different situations. However, no consensus has been reached on their underlying mechanism, and diverse interpretations have been proposed. For instance, it has been suggested that the sign of the like-charged particle interactions can be reversed from repulsive to attractive by wall effects [1,2], particle dipole moments [3], surface tension [4–7], nonequilibrium hydrodynamical effects [8–11], or external electromagnetic fields [12–16]. Generally, understanding the attraction between charged colloidal particles in solutions requires detailed knowledge of charge distribution in the system, which is extremely difficult to obtain experimentally or theoretically.

On the other hand, in crystalline solids, defects such as dislocations, interstitials, and vacancies, are often expelled from crystalline domains [17,18], and concentrate in areas near the grain boundaries [19,20]. The aggregation of defects implies an apparent attraction between isolated defects in crystals [17,21–28], whose origin can be attributed to the thermodynamic requirement of reducing the overall lattice distortion in the system. It is reasonable to expect that similar induced attractions may exist between diffusing like-charged intruders that only transiently perturb the background lattice, instead of permanently distorting it to form defects. Such cases are reminiscent of the phonon-mediated attractions between electrons in Cooper pairs in superconductors [29,30], where the background ions remain on lattice sites when averaged over time.

In this Letter, we report the observation of effective attractions between small diffusing like-charged colloidal tracers in a background of quasi-two-dimensional (quasi-2D) colloidal crystals. Using a counting method which properly takes into account the configurational degeneracy of the relative positions of tracers, we show that the probability of two tracers locating in the nearest-neighbor cells of the crystalline background is much higher than the probabilities at greater separations. The intensity of this effective attraction depends sensitively on the lattice constants of the crystalline background. The mechanism of this lattice-induced effective attraction is elucidated by comparing the relative probability of tracer configurations and the free energy cost from lattice deformations.

Experiments.—The samples consist of a bidisperse aqueous solution of polystyrene (PS) particles with the diameters of $\sigma_s = 0.2$ μm for small tracer particles and $\sigma_l \simeq 4\sigma_s$ for large particles. The mean number ratio between the large and small particles is 100∶1. The large particles are negatively charged by sulfonation in sulfuric acid [31], and the interparticle repulsion distances can be tuned by varying the sulfonation time and the quantity of the sulfuric acid (see the Supplemental Material for more details [32]). The small tracer particles are negatively charged with anionic carboxyl groups and fluorescently labeled. The samples are hermetically sealed between two negatively charged cover slides, forming a tightly confined quasi-two-dimensional system. The buckling of background particles, which has been reported in less confined colloidal crystals,

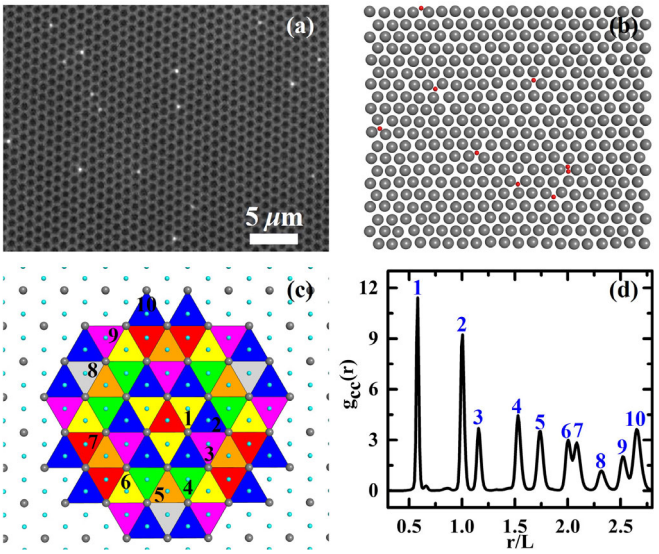

FIG. 1. (a) Experimental snapshot of the tracer particles diffusing in a background of quasi-two-dimensional colloidal crystal, in which the bright particles are small fluorescent probe particles. (b) Sketch of simulation system, consisting of red small tracers and a crystalline lattice background. (c) Schematic diagram for determining the neighboring cells with respect to the red triangle in the center of simulation system. The large grey particles correspond to the background particles, and the small cyan beads are the centers of triangular cells. Neighbors from 1 to 10 are marked by digits and different colors. (d) The measured pair correlation function of the triangular cell centers of the lattice corresponding to (a). Different neighboring cells are determined by the location of peaks marked by blue digits.

is thus avoided [33,34]. The large PS particles form a monolayer of triangular lattice, in which the strong repulsion between the PS particles creates interparticle gaps wide enough for the small tracers to diffuse through. In experiments, we employ four types of charged particles with different charge densities to obtain crystalline backgrounds with lattice constants from 0.869 μm to 4.429 μm. The interactions between all the particles used in the experiments can be found in the Supplemental Material [32]. The images of samples are acquired by video microscopy in a combined bright field and fluorescent mode with an oil-immersed $\times 100$ objective at 55 frames/s. Figure 1(a) shows a snapshot of the sample image in experiment. The positions of all particles are extracted using particle tracking techniques [35].

Simulation.—In simulations, we consider a few small tracers of diameter σ_s diffusing in a two-dimensional lattice background composed of 400 large particles with the diameter $\sigma_l = 4\sigma_s$, as sketched in Fig. 1(b). A Weeks-Chandler-Andersen–type of potential $U_{\mathrm{LJ}}(r) = 4\epsilon[(\sigma/r)^{2n} - (\sigma/r)^n] + \epsilon$ is used to describe the repulsive interactions between all particles, unless otherwise stated. Here, the interaction intensity is taken as $\epsilon = k_B T = 1$, the interaction diameter between the large and small particles is taken as $\sigma = (\sigma_l + \sigma_s)/2$, and n is the potential stiffness. The dynamics of all particles is described by the overdamped Langevin equation $\gamma \mathbf{v} = \mathbf{F}_r + \boldsymbol{\eta}$ with periodic boundary conditions, where γ refers to the friction coefficient, $\mathbf{F}_r$ to the steric interaction force, and $\boldsymbol{\eta}$ to the Gaussian distributed stochastic force with $\langle \boldsymbol{\eta} \rangle = 0$ and $\langle \eta_i(t)\eta_j(t') \rangle = 2k_B T\gamma\delta_{ij}\delta(t - t')$.

Results and discussion.—During the experiment, the tracers diffuse in the triangular lattice matrix formed by the background particles. To determine the effect of the fluctuating background lattice on the effective interactions between the diffusing tracers, we measure the probability of finding a tracer pair in triangular lattice cells with different separations (see the Supplemental Material for details of how to determine the triangular cell that a tracer particle locates in [32]). For any reference cell in the lattice [red cell in Fig. 1(c)], there exist neighboring cells that are equivalently positioned [identically colored cells in Fig. 1(c)]. These equivalent cells can be determined by their center-to-center distance to the reference cell. Figure 1(d) plots the pair correlation function $g_{cc}(r)$ of the cell centers in the experiments. Each peak indicates a set of equivalent neighboring cells. The number of each set of equivalent cells, which depends on the distance to the reference cell, is the "degeneracy" of the cell pairs that needs to be taken into account when evaluating the relative probability of finding tracer pairs in certain pair of lattice cells.

Figure 2(a) plots the relative probability

$$P(m) = \frac{\sum_{i\in m} \frac{1}{g_{ss}(r)} / \sum_{i\in 1,\ldots,10} \frac{1}{g_{ss}(r)}}{D(m) / \sum_{m=1}^{10} D(m)} \tag{1}$$

of finding a tracer pair in the mth nearest neighbor cell. The probability is normalized by the cell degeneracy $D(m)$ and pair correlation function $g_{ss}(r)$ of the tracer particles measured in dilute solutions without the background lattice. The latter normalization is necessary to deduct the effect of the direct interactions between the tracers by multiplying a factor of $1/g_{ss}(r)$ to the countings of tracer pairs with separation r so that $P = 1$ if the distribution of the small tracers is not affected by the background lattice. $P > 1$ corresponds to a higher probability of finding a tracer pair in certain neighbor cells than the probability determined by the tracer interactions alone, indicating additional interactions (see the Supplemental Material for the derivation of $P(m)$ [32]). For small lattice constants ($L = 0.869$ μm and 1.041 μm), the relative probability is significantly greater than unity at the first neighbor cell, while remains close to 1 at longer distances, indicating a lattice-induced short-range attraction between the repulsive tracers. This attraction decreases rapidly with the lattice constants. For $L =$ 2.105 μm and 4.429 μm, no enhanced P is observed at all neighbor cells. The probability values for cell number 6 to 7 and 9 to 10 are missing due to merged $g_{cc}(r)$ peaks for the background lattices in the two samples, which originates from the slightly decrease of the lattice quality

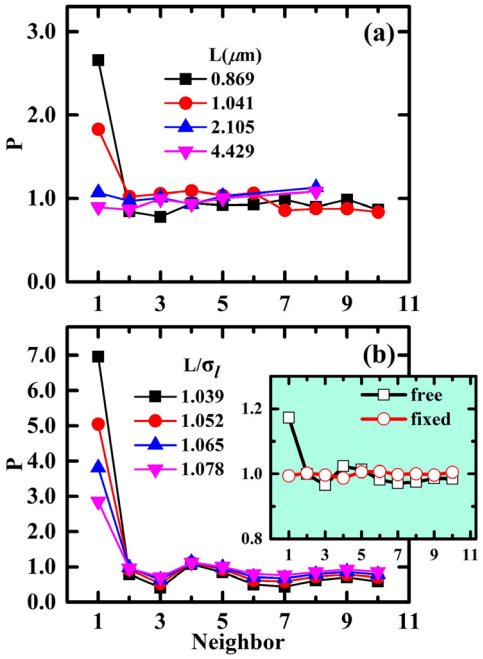

FIG. 2. Relative probabilities of finding a tracer pair in neighbor cells from 1 to 10 by experiments (a) and simulations (b). The stiffness of potential interactions in simulations is $n_{ll} = 12$ between background particles and $n_{ls} = 12$ between tracer and background particles, and a soft repulsive potential between tracers extracted from experiment is used for consistency. The lower inset compares the relative probability in the fluctuating background with that in the fixed background, in which the lattice constant L/σ_l is 1.078, the stiffness parameters are $n_{ll} = 12$, $n_{ls} = 12$, $n_{ss} = 2$, and the interaction diameter between large and small particles is taken as $0.88 \times (\sigma_l + \sigma_s)/2$.

due to the particle softness. In experiments and simulations, $P(m)$ is measured up to the 10th shell, as the value of P rapidly reaches a constant beyond the first few neighbor cells.

We emphasize that the discrete relative probability P at different cell separations, instead of the commonly used pair correlation function $g(r)$, correctly characterizes the effective interactions between tracers in a crystalline background. This is because the tracer $g(r)$, which is generally obtained on the basis of isotropic and homogeneous condition, may indicate artificial attraction in the lattice background [36–40] (see the Supplemental Material [32]).

The lattice-induced attraction between like-charged tracers is confirmed by Brownian dynamics simulations. For consistency with the experiment, we use a repulsive soft potential to describe the interactions between small tracers, which is obtained from the experiments in dilute solutions absent of any large background particles. Figure 2(b) plots the measured relative probability at different neighbor cells from simulations. For all four lattice constants studied, a pronounced peak is observed in the first neighbor cell, while P remains flat for neighboring cells at larger separations. This short-range attraction decreases rapidly as the background lattice constant increases, consistent with the observations in experiments. The relative probability P at large separations (e.g., cell number 9 or 10) is less than 1, as the countings in these cells are reduced due to the relatively large number of countings for the first neighbor cells. To determine the influence of the lattice fluctuations on the observed effective attraction, we compare the relative probability P obtained in a frozen triangular lattice and a thermally fluctuating lattice. For both systems, the background lattice constant is chosen to be $L/\sigma_l = 1.078$ and the interaction diameter between the large and small particles is $0.88 \times (\sigma_l + \sigma_s)/2$, so that the tracers can easily diffuse even in the frozen background. The measured relative probabilities from the two systems are plotted in the inset of Fig. 2(b). No attraction is observed in the frozen lattice, while $P \approx 1.2$, well above the noise level, is obtained in the first neighbor cell for the fluctuating lattice. The absence of apparent attractions in frozen lattices suggests that the observed attractions between tracers are indeed induced by the fluctuating background lattice.

Microscopically, the origin of the effective attractions between tracers can be attributed to the lattice distortion caused by the tracers, and the associated free energy changes. The presence of a tracer in a triangular cell in the background distorts the shape of the cell, creating a penalty for elastic energy. It also reduces the volume accessible to the background particles, thereby reducing the vibrational entropy of the majority particles. As a result, the system tends to reduce its total free energy cost by pushing two tracer particles into the nearest neighbor cells. Assuming the presence of a tracer elongates the bond closest to it from x to $d = x + \delta x$, as illustrated in Fig. 3(a), the system free energy cost can be nearly halved by moving two distant tracers into neighboring cells that share an elongated bond.

The free energy differences between the two local configurations depicted in Fig. 3(a) are quantitatively determined by simulations. We first measure the force needed to extend a certain bond by δx, which are obtained by applying two forces of the same magnitude in opposite directions on two adjacent background particles forming a bond. Figure 3(b) plots the force f as a function of lattice extension for four different lattice constants. The force required to extend the bond length is considerably higher for lattices with smaller lattice constants. For an isothermal and reversible thermal process, the increment of free energy ΔF equals the external work ΔW on the system. The free energy increase ΔF for an elongated bond is thus the integral of f over δx. The integral limits, which are indicated by colored arrows in Fig. 3(b), are obtained by measuring the bond length extension closest to a tracer in the simulations. The free energy difference between the two configurations is associated with their probabilities by $P(1)/P(\infty) = e^{\Delta F/k_B T}$, where $P(1)$ is the probability of finding two tracers in the nearest neighbor cells, and $P(\infty)$ is the probability of finding them in large separations.

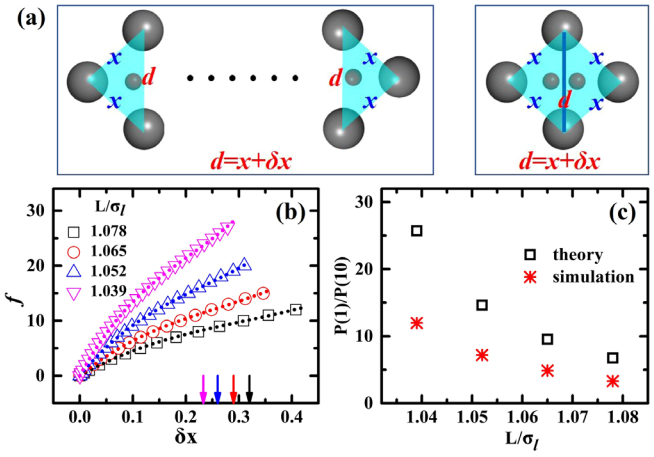

FIG. 3. (a) Schematic diagram of the lattice distortion. The bond length is elongated to $d = x + \delta x$ from x due to the invasion of the tracer, and two elongated bonds merge into one when two tracer particles are located in the nearest-neighbor cells. (b) Drag force f as a function of elongated distance δx between two large background particles for various lattice constants L/σ_l. Dotted lines are fits to the simulation data, and the arrows to the x axis are the corresponding integral limits for work calculation. The stiffness parameters are $n_{ll} = 12$ and $n_{ls} = 12$. (c) The probability ratio of two particles in the first to the tenth nearest-neighbor cells obtained from theory and simulation.

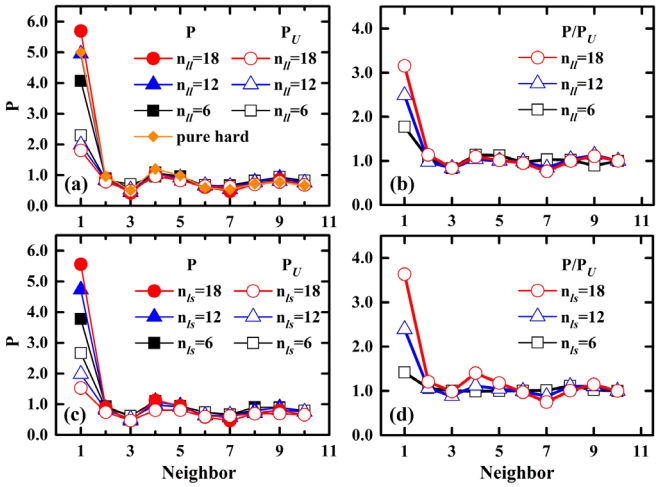

FIG. 4. Relative probabilities P (solid symbols) and the contributions from the elastic energy P_U (open symbols) for different stiffnesses of potential interactions (a) between background particles n_{ll} and (c) between tracer and background particles n_{ls}. The orange curve in (a) is obtained in the pure hard spheres system by Monte Carlo simulations (see the Supplemental Material for the simulation details [32]). Here, the reference parameters are $n_{ll} = 12$, $n_{ls} = 12$, $n_{ss} = 2$, and $L/\sigma_l = 1.052$. (b) and (d) show the entropy contributions to the relative probabilities, P/P_U, corresponding to (a) and (c), respectively.

For practical purposes, we choose $P(10) \approx P(\infty)$. Figure 3(c) plots the probability ratio $P(1)/P(10)$ as a function of lattice constant. The theoretical values of the ratio $P(1)/P(10)$ obtained from ΔF, agree semiquantitatively with direct measurements in the simulations. The theoretical model slightly overestimates the $P(1)/P(10)$ ratio, as the bond shared by the two cells each containing a tracer particle is likely extended more than δx, thus reducing the free energy difference between the two configurations. In addition, the above calculation does not consider the possible distortion of other bonds of the related cells in Fig. 3(a), which may further reduce ΔF.

We further identify the contributions from elastic energy and entropy in the system free energy to the observed effective attraction. In canonical ensembles, the probability of finding two tracers in the mth nearest neighbor cells, normalized by the configurational degeneracy, is $P(m) \propto \exp[-F_m/k_BT]$, where $F_m = -k_BT \times \ln\{\int \exp[-U(\boldsymbol{r}^N|m\text{th cells})/k_BT)]d\boldsymbol{r}^N\}$ is the Helmholtz free energy of the system in the subensemble where the two tracers are located in the mth nearest neighbor cells. Accordingly, the internal energy U_m and entropy S_m can be defined under the same constraints, with $F_m = U_m - TS_m$. In the simulations, the overall probability $P(m)$ is directly measured, and U_m can be obtained by averaging the internal energy over all the configurations with two tracers in the mth neighboring cells, with $P_U(m) \propto \exp[-U_m/k_BT]$. The contribution to the overall probability from the entropy term is thus $P(m)/P_U(m)$.

Figure 4 plots $P(m)$, $P_U(m)$, and $P(m)/P_U(m)$ for various stiffnesses of interparticle interactions. The stiffness is tuned by changing the power index n of the Weeks-Chandler-Andersen type of potential, with larger n indicating stiffer potentials. The overall P(1), and hence the attraction increases with the stiffness of interactions between particles, similar to the phonon-mediated attractions between electrons in some superconductors [41,42]. The contributions from the energy term decrease with the system stiffness, while the entropy contribution increases with n. As shown by the orange curve in Fig. 4(a), this induced attraction can also be found in hard-sphere systems, where it is driven solely by entropy. Thus in the hard sphere limit, these effective interactions between the small tracers can be viewed as a new type of entropic (or depletion) force. And in this case, the depletants are the large background particles vibrating on lattice sites that collectively gain additional vibrational entropy by pushing two smaller tracers into the nearest neighbor cells, in contrast to conventional depletion forces in colloids where the depletants are usually free-diffusing small particles [43–46].

Conclusion.—We observe apparent short-range attractive interactions between like-charged tracers diffusing in triangular colloidal backgrounds at two dimensions, using both microscopy experiments and simulations. Such effective attractions are fundamentally different from previously reported like-charge attractions between colloidal particles, and is of thermodynamical origin with strong contributions from entropy. This type of entropic force enriches the

existing picture of the depletion interaction that traditionally occurs only in a colloidal fluid background. When properly tuned, such lattice induced attractions between colloidal particles may be employed to direct the assembly of microdevices or to sort colloidal particles of different sizes or chemical properties. Moreover, the like-charged tracer attraction mediated by the fluctuating lattice also shows an interesting similarity to electron Cooper pairs in superconductors, highlighting the ubiquity of this phenomenon.

We thank Rui Liu for helpful discussions. We acknowledge the support of the National Natural Science Foundation of China (Grants No. 12174434, No. 11874395, No. 11874397, No. 11674365, and No. 12047552). This work was also supported by the Strategic Priority Research Program of Chinese Academy of Sciences (Grant No. XDB33000000).

P. L. and L. N. contributed equally to this work.

*fye@iphy.ac.cn
†mcyang@iphy.ac.cn
‡kechen@iphy.ac.cn

[1] D. G. Grier, Nature (London) **393**, 621 (1998).
[2] Y. Han and D. G. Grier, Phys. Rev. Lett. **91**, 038302 (2003).
[3] W. Chen, S. Tan, T.-K. Ng, W. T. Ford, and P. Tong, Phys. Rev. Lett. **95**, 218301 (2005).
[4] M. Oettel and S. Dietrich, Langmuir **24**, 1425 (2008).
[5] W. Fei, Y. Gu, and K. J. M. Bishop, Curr. Opin. Colloid Interface Sci. **32**, 57 (2017).
[6] L. Wu, X. Wang, G. Wang, and G. Chen, Nat. Commun. **9**, 1335 (2018).
[7] S. E. Rahman, N. Laal-Dehghani, S. Barman, and G. F. Christopher, J. Colloid Interface Sci. **536**, 30 (2019).
[8] T. M. Squires and M. P. Brenner, Phys. Rev. Lett. **85**, 4976 (2000).
[9] F. Martínez-Pedrero and P. Tierno, J. Colloid Interface Sci. **519**, 296 (2018).
[10] A. Théry, L. Le Nagard, J.-C. Ono-dit Biot, C. Fradin, K. Dalnoki-Veress, and E. Lauga, Sci. Rep. **10**, 13578 (2020).
[11] T. A. Witten and H. Diamant, Rep. Prog. Phys. **83**, 116601 (2020).
[12] K. A. Komarov, N. P. Kryuchkov, and S. O. Yurchenko, Soft Matter **14**, 9657 (2018).
[13] E. V. Yakovlev, M. Chaudhuri, N. P. Kryuchkov, P. V. Ovcharov, A. V. Sapelkin, and S. O. Yurchenko, J. Chem. Phys. **151**, 114502 (2019).
[14] K. A. Komarov, A. V. Yarkov, and S. O. Yurchenko, J. Chem. Phys. **151**, 244103 (2019).
[15] K. A. Komarov and S. O. Yurchenko, Soft Matter **16**, 8155 (2020).
[16] A. Spatafora-Salazar, D. M. Lobmeyer, L. H. P. Cunha, K. Joshi, and S. L. Biswal, Soft Matter **17**, 1120 (2021).
[17] W. Lechner and C. Dellago, Soft Matter **5**, 2752 (2009).
[18] W. Lechner, D. Polster, G. Maret, P. Keim, and C. Dellago, Phys. Rev. E **88**, 060402(R) (2013).
[19] K. Yoshizawa, A. Toyotama, T. Okuzono, and J. Yamanaka, Soft Matter **10**, 3357 (2014).
[20] A. Toyotama, T. Okuzono, and J. Yamanaka, Sci. Rep. **6**, 23292 (2016).
[21] A. Pertsinidis and X. S. Ling, Phys. Rev. Lett. **87**, 098303 (2001).
[22] C. Eisenmann, U. Gasser, P. Keim, G. Maret, and H.-H. von Grünberg, Phys. Rev. Lett. **95**, 185502 (2005).
[23] P. N. Ma, L. Pollet, M. Troyer, and F. C. Zhang, J. Low Temp. Phys. **152**, 156 (2008).
[24] U. Gasser, C. Eisenmann, G. Maret, and P. Keim, Chem. Phys. Chem. **11**, 963 (2010).
[25] B. He and Y. Chen, Solid State Commun. **159**, 60 (2013).
[26] W. Lechner, H.-P. Büchler, and P. Zoller, Phys. Rev. Lett. **112**, 255301 (2014).
[27] W. Lechner, F. Cinti, and G. Pupillo, Phys. Rev. A **92**, 053625 (2015).
[28] Z. Han, L. Zhang, C. Wang, X. Ni, B. Ye, and L. Shi, Vacuum **180**, 109583 (2020).
[29] J. Bardeen, L. N. Cooper, and J. R. Schrieffer, Phys. Rev. **108**, 1175 (1957).
[30] J. Linder and A. V. Balatsky, Rev. Mod. Phys. **91**, 045005 (2019).
[31] M. Hazarika, K. Malkappa, and T. Jana, Polym. Int. **61**, 1425 (2012).
[32] See Supplemental Material at http://link.aps.org/supplemental/10.1103/PhysRevLett.129.018002 for additional experimental and simulation details, which includes Refs. [2,3].
[33] Y. Han, Y. Shokef, A. M. Alsayed, P. Yunker, T. C. Lubensky, and A. G. Yodh, Nature (London) **456**, 898 (2008).
[34] E. Janai, A. V. Butenko, A. B. Schofield, and E. Sloutskin, Soft Matter **15**, 5227 (2019).
[35] J. C. Crocker and D. G. Grier, J. Colloid Interface Sci. **179**, 298 (1996).
[36] G. Cruz de León, J. M. Saucedo-Solorio, and J. L. Arauz-Lara, Phys. Rev. Lett. **81**, 1122 (1998).
[37] G. Cruz de León and J. L. Arauz-Lara, Phys. Rev. E **59**, 4203 (1999).
[38] S. Sokolowski, W. Rzysko, and O. Pizio, J. Colloid Interface Sci. **218**, 341 (1999).
[39] W. Rzysko, O. Pizio, and S. Sokolowski, Physica (Amsterdam) **273A**, 241 (1999).
[40] M. Mayorga, C. Corona, C. Sandoval, and O. Pizio, Czech. J. Phys. **50**, 727 (2000).
[41] G. Grimvall, *The Electron-Phonon Interaction in Metals* (North-Holland Publishing Company, 1981).
[42] L. P. Gor'kov and V. Z. Kresin, Rev. Mod. Phys. **90**, 011001 (2018).
[43] T. Biben, P. Bladon, and D. Frenkel, J. Phys. Condens. Matter **8**, 10799 (1996).
[44] A. Stradner, H. Sedgwick, F. Cardinaux, W. C. K. Poon, S. U. Egelhaaf, and P. Schurtenberger, Nature (London) **432**, 492 (2004).
[45] S. Sacanna, W. T. M. Irvine, P. M. Chaikin, and D. J. Pine, Nature (London) **464**, 575 (2010).
[46] M. D. Gratale, T. Still, C. Matyas, Z. S. Davidson, S. Lobel, P. J. Collings, and A. G. Yodh, Phys. Rev. E **93**, 050601(R) (2016).